

PHASE MIXING IN MOND

L. CIOTTI* and C. NIPOTI

*Dept. of Astronomy, University of Bologna,
via Ranzani 1, I-40127, Bologna, Italy*

**E-mail: luca.ciotti@unibo.it*

P. LONDRILLO

*INAF - Bologna Astronomical Observatory,
via Ranzani 1, I-40127, Bologna, Italy*

Dissipationless collapses in Modified Newtonian Dynamics (MOND) have been studied¹ by using our MOND particle-mesh N-body code, finding that the projected density profiles of the final virialized systems are well described by Sersic profiles with index $m \lesssim 4$ (down to $m \sim 2$ for a deep-MOND collapse). The simulations provided also strong evidence that phase mixing is much less effective in MOND than in Newtonian gravity. Here we describe “ad hoc” numerical simulations with the force angular components frozen to zero, thus producing radial collapses. Our previous findings are confirmed, indicating that possible differences in radial orbit instability under Newtonian and MOND gravity are not relevant in the present context.

Keywords: gravitation — stellar dynamics — methods: numerical

1. Introduction

In the Lagrangian formulation of Milgrom’s Modified Newtonian Dynamics (MOND)^{2,3} the Poisson equation $\nabla^2 \phi_N = 4\pi G \rho$ for the Newtonian potential ϕ_N is replaced by the field equation for the MOND potential ϕ

$$\nabla \cdot [\mu (\|\nabla \phi\|/a_0) \nabla \phi] = 4\pi G \rho, \quad (1)$$

where ρ is the density distribution, $a_0 \simeq 1.2 \times 10^{-10} \text{m s}^{-2}$ is a characteristic acceleration, $\|\dots\|$ is the standard Euclidean norm, and in finite mass

systems $\nabla\phi \rightarrow 0$ for $\|\mathbf{x}\| \rightarrow \infty$. The MOND gravitational field experienced by a test particle is $\mathbf{g} = -\nabla\phi$, and $\mu(y) \sim y$ for $y \ll 1$ and ~ 1 for $y \gg 1$ (typically $\mu = y/\sqrt{1+y^2}$). In the ‘deep MOND regime’ describing low-acceleration systems ($\|\nabla\phi\| \ll a_0$, hereafter dMOND), $\mu(y) = y$ and so Eq. (1) simplifies to $\nabla \cdot (\|\nabla\phi\|\nabla\phi) = 4\pi G a_0 \rho$. The source term in Eq. (1) can be eliminated by using the Poisson equation, giving

$$\mu(\|\nabla\phi\|/a_0)\nabla\phi = \nabla\phi_N + \mathbf{S}, \quad (2)$$

where \mathbf{S} is a solenoidal field dependent on ρ and in general different from zero; when $\mathbf{S} = 0$ Eq. (2) can be solved explicitly in terms of $\nabla\phi_N$. This reduction would be most useful for numerical simulations. Unfortunately $\mathbf{S} = 0$ only for very special^{2,4} configurations. In addition, though the field \mathbf{S} has been shown to be small^{4,5} for some configurations, neglecting it when simulating time-dependent dynamical processes has dramatic effects such as non-conservation⁶ of the total linear momentum.

Several astronomical observational data appear consistent^{7,8} with the MOND hypothesis, and also a relativistic version⁹ of MOND is now available, making it an interesting alternative to the cold dark matter paradigm. However, dynamical processes in MOND have been investigated very little¹⁰⁻¹⁴ so far, mainly due to difficulties posed by the non-linearity of Eq. (1). In a recent paper¹ (hereafter NLC) we presented the results of N-body simulations of *dissipationless collapse* in MOND obtained with our N-body code which solves Eq. (1) exactly. In particular, we obtained clear indications that *phase mixing* is much less effective in MOND than in Newtonian gravity. Here, after summarizing the main results of NLC, and restricting for simplicity to the Newtonian and dMOND regimes only, we address the problem of the importance of the force angular components in the relaxation process, by running ‘ad hoc’ numerical simulations with the force angular components frozen to zero.

2. The N-body code and the numerical simulations

Our MOND N-body code^{1,5} is based on a particle-mesh scheme with quadratic spline interpolations. The spherical grid on which Eq. (1) is solved

is made of $N_r \times N_\vartheta \times N_\varphi$ points. We use leap-frog time integration, where the adaptive time-step is the same for all particles. All the computations on the particles and the particle-mesh interpolations can be split among different processors, while the iterative potential solver computations are not performed in parallel: however, at each time step we can use the potential previously determined as seed solution. We successfully tested the code by running Newtonian simulations (i.e., by solving Eq. [1] in the limit $\mu = 1$), and comparing the results with those of simulations performed with our FVFPS^{15,16} treecode starting from the same initial conditions. We also verified that the code reproduces the Newtonian and MOND conservation laws. In fact, $2K + W = 0$ for virialized systems in MOND and in Newtonian gravity, where K is the total kinetic energy and $W = \text{Tr } W_{ij}$ is the trace of the potential energy tensor^{17,18}

$$W_{ij} \equiv - \int \rho(\mathbf{x}) x_i \frac{\partial \phi(\mathbf{x})}{\partial x_j} d^3 \mathbf{x}. \quad (3)$$

Note that in MOND $K + W$ is *not* the total energy, and is not conserved. However, W is conserved in the limit of dMOND, being $W(t) = -(2/3)\sqrt{Ga_0 M_*^3}$ for all systems^{1,19-21} of finite total mass M_* .

The choice of appropriate scaling physical units is an important aspect of MOND N-body simulations. A full discussion of this point can be found in NLC; here we just recall that, while in Newtonian simulations the natural scaling units are $t_{*n} = r_*^{3/2}(GM_*)^{-1/2}$, $v_{*n} = (GM_*)^{1/2}r_*^{-1/2}$, and $E_{*n} = GM_*^2 r_*^{-1}$, in the dMOND case one has $t_{*d} = r_*(GM_* a_0)^{-1/4}$, $v_{*d} = (GM_* a_0)^{1/4}$, and $E_{*d} = (Ga_0)^{1/2} M_*^{3/2}$, where r_* and M_* are the length and mass units in which the initial conditions are expressed. In NLC we performed a set of N-body simulations of dissipationless collapses, starting from the same phase-space configuration, i.e., from a cold ($2K/|W| = 0$) Plummer²² sphere of total mass M_* and “core” radius r_* . The gravitational potential is Newtonian in simulation N and dMOND in simulation D; the full MOND simulations are not described here (see NLC). All the simulations ($N = 10^6$ particles, $N_r = 64$, $N_\vartheta = 16$ and $N_\varphi = 32$) are evolved up to $t = 150t_{\text{dyn}}$, where t_{dyn} is defined as the time at which $2K/|W|$ reaches its maximum value ($t_{\text{dyn}} \sim 2t_{*d}$ in simulation D, and $\sim 2t_{*n}$ in N). The

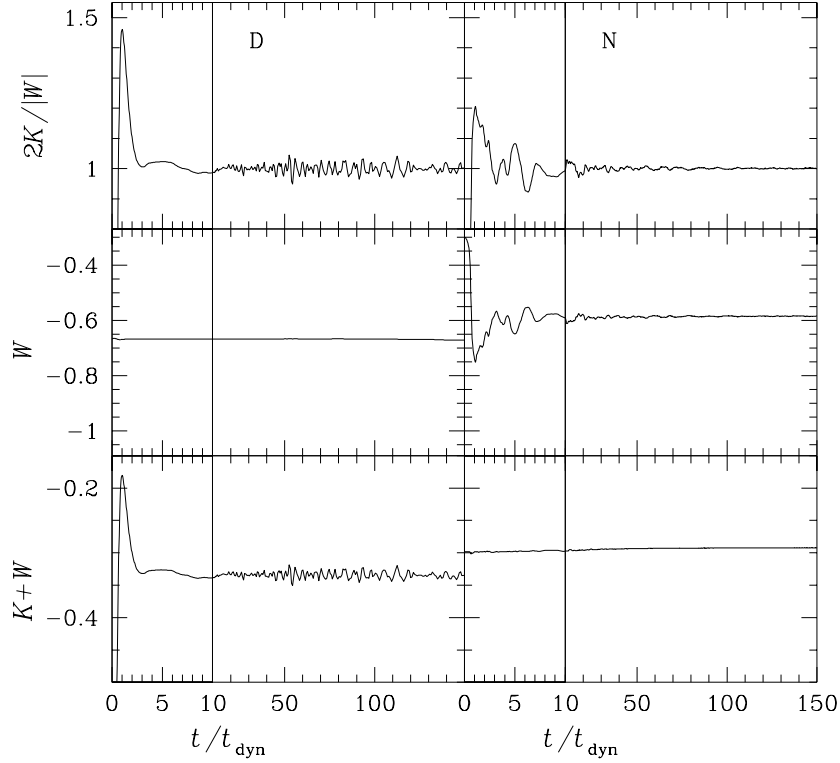


Fig. 1. Time evolution of $2K/|W|$, W , and $K+W$ for a dMOND (D) and a Newtonian (N) simulation. K , W , and $K+W$ are in units of E_{*d} (D), and E_{*n} (N). Note the long-lasting oscillations of the virial ratio in D.

center of mass, and the modulus of the total angular momentum (in units of $r_*M_*v_{*n}$ for model N and of $r_*M_*v_{*d}$ for model D) oscillates around zero with r.m.s. $\lesssim 0.1r_*$ and $\lesssim 0.02$, respectively. The quantities $K+W$ in simulation N, and W in simulation D are conserved to within 2% and 0.6%, respectively (see Fig.1). The final angle-averaged density profiles are fitted with a γ -model^{25,26}

$$\rho(r) = \frac{(3-\gamma)M_*r_c}{4\pi r^\gamma(r_c+r)^{4-\gamma}}; \quad (4)$$

for each end-product we also measure the axis ratios c/a and b/a of the

inertia ellipsoid^{23,24} ($a \geq b \geq c$), the ellipticity ϵ of the projections along the principal axis, and the corresponding circularized effective radius R_e . The resulting circularized projected density profiles are fitted with the Sersic^{27,28} law

$$I(R) = I(R_e) e^{-b(m)[(R/R_e)^{1/m} - 1]}, \quad (5)$$

where²⁹ $b(m) \simeq 2m - 1/3 + 4/405m$. Note that m is the only free parameter, because R_e and $I(R_e)$ are fixed by particle count.

3. Results

3.1. Structure and kinematics of the collapse end-products

All the final virialized systems in NLC depart significantly from spherical symmetry. In particular, the D end-product is triaxial ($c/a \sim 0.2$, $b/a \sim 0.4$; $0.5 \lesssim \epsilon \lesssim 0.8$), while model N is oblate ($c/a \sim c/b \sim 0.5$; $0 \lesssim \epsilon \lesssim 0.5$). These values are consistent with those observed in real ellipticals, with the exception of model D, which would correspond to an E8 galaxy. Thus, MOND gravity could be able to produce some system that would be unstable in Newtonian gravity. The final angle-averaged density of model N is well described by Eq. (4) with $\gamma \sim 1.7$, while $\gamma \sim 0$ in model D. Equation (5) fits remarkably well the final surface density profiles (best-fit index $m \sim 4$ in model N, and $m \sim 2$ in D, see Table 2 in NLC), with average residuals $0.05 \lesssim \langle \Delta SB \rangle \lesssim 0.2$, where $SB \equiv -2.5 \log[I(R)/I(R_e)]$. Note that the fitting radial range $0.1 \lesssim R/R_e \lesssim 10$ is comparable with or larger than the typical ranges³⁰ spanned by observations. The internal kinematics of the end-products is quantified by the angle-averaged radial and tangential components of their velocity-dispersion tensor (σ_r and σ_t), and by the anisotropy parameter $\beta(r) \equiv 1 - 0.5\sigma_t^2/\sigma_r^2$. All systems are strongly radially anisotropic outside the half-mass radius. The σ_r profile decreases steeply in the final state of model N, while it presents a hole in the inner regions of model D. In addition, model D is radially anisotropic ($\beta \sim 0.4$) even in the central regions, where model N is approximately isotropic ($\beta \sim 0.1$). The line-of-sight velocity dispersion σ_{los} declines steeply within R_e in model N, while the D profile is significantly flatter.

3.2. Phase-space properties

In Newtonian gravity, collisionless systems virialize through violent relaxation in few dynamical times, as predicted by the theory³¹ and confirmed by numerical^{24,32} simulations. Due to the non linearity of the theory, the details of relaxation processes and virialization in MOND are much less known. In Fig. 1 we show the time evolution of $2K/|W|$, W , and $K + W$ for simulations D and N of NLC. In simulation N, $2K/|W|$ has a peak, then oscillates, and eventually converges to the equilibrium value 1; the total energy $K + W$ is nicely conserved. The time evolution is significantly different in simulation D, where W is constant as expected, but $2K/|W|$ *still oscillates at very late times* because of the oscillations of K . A different view of phase space is given in Fig. 2, where we plot time snapshots of the particles radial velocity vs. radius for simulations D and N. At $t = t_{\text{dyn}}$ (time of the peak of $2K/|W|$), sharp shells in phase space are present, indicating that particles are moving in and out collectively and phase mixing has not taken place yet. At significantly late times ($t = 44t_{\text{dyn}}$), when the systems are almost virialized ($2K/|W| \sim 1$), phase mixing is complete in simulation N, but phase space shells still survive in model D. Finally, the bottom panels show the (r, v_r) plane at equilibrium ($t = 150t_{\text{dyn}}$), when phase mixing is completed also in model D: note how the populated regions are significantly different for the two models. Thus, NLC results indicate that phase mixing is more effective in Newtonian gravity than in MOND. *Here we address the issue of the importance of the force angular components during the collapse. In fact, one could speculate that a different behavior of radial orbit instability in MOND and in Newtonian gravity could be at the origin of the different time scale of phase mixing.* As shown in Fig.3, also the new simulations confirm that phase mixing is less effective in MOND than in Newtonian gravity (even though virialization times are now longer than in NLC models, due to the reduced number of active degrees of freedom).

In NLC we obtained additional information on the relaxation process from the differential energy distribution¹⁷ $N(E)$ (i.e. the number of particles with energy per unit mass between E and $E+dE$). In Newtonian gravity ϕ is

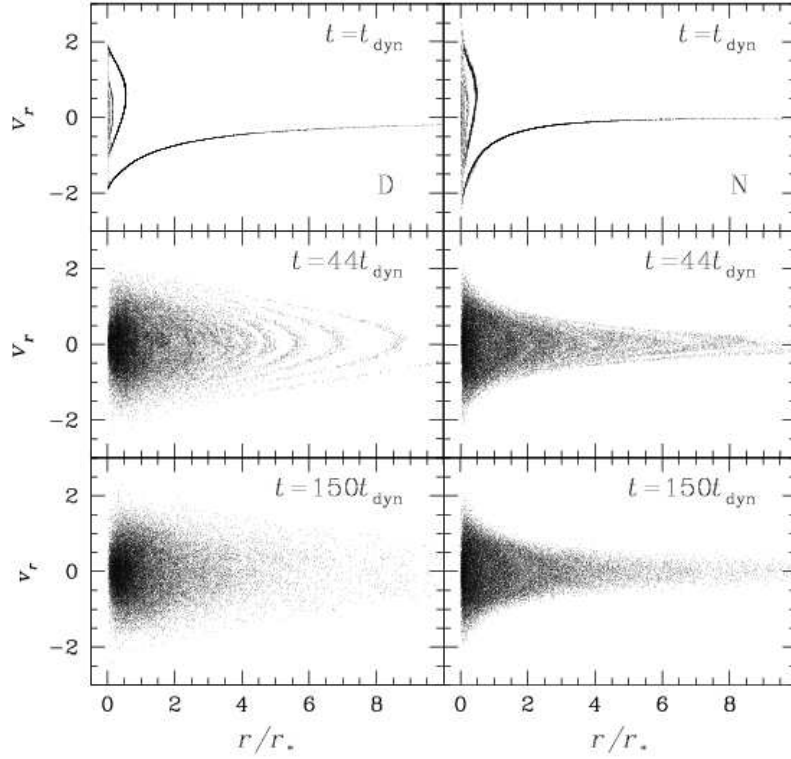


Fig. 2. Radial-velocity vs. radius of 32000 particles randomly extracted from simulations D and N. v_r is in units of v_{*d} (D) or v_{*n} (N).

usually set to zero at infinity for finite-mass systems, so $E = v^2/2 + \phi(\mathbf{x}) < 0$ for bound particles; in MOND all particles are bound independently of their velocity, because ϕ is confining, and all energies are admissible (see Fig. 5 of NLC). Given that the particles are at rest at $t = 0$, the initial $N(E)$ depends only $\phi(\mathbf{x})$ at $t = 0$, and it is significantly different in the Newtonian and MOND cases. In accordance with previous studies, we found that in the Newtonian case the final $N(E)$ is well represented by an exponential function^{24,28,32–35} over most of the populated energy range. In contrast, in model D the final $N(E)$ decreases for increasing energy, qualitatively pre-

serving its initial shape. We interpret this result as another manifestation of a less effective phase space reorganization in MOND than in Newtonian collapses.

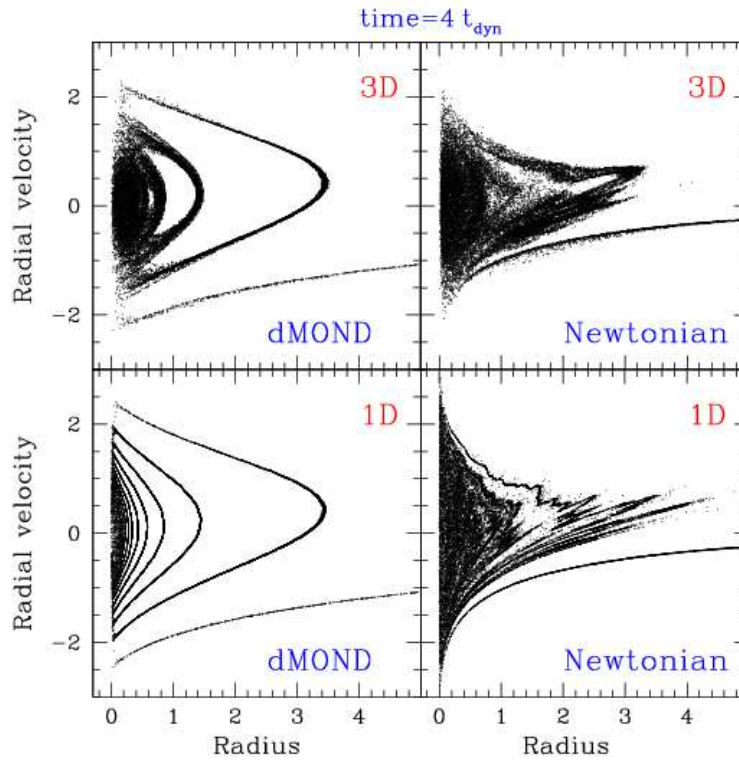


Fig. 3. Phase space sections for simulations with frozen angular force components (bottom panels), and with the three force components active (top panels).

4. Conclusions

We presented results of dissipationless collapses in MOND, focusing on the relaxation process. The main results can be summarized as follows:

1) Newtonian collapses produced cuspiest density profiles than MOND simulations ($\gamma \sim 1.7$ and $m \sim 4$ vs. $\gamma \sim 0$ and $m \sim 2$). In both cases

the Sersic fits are remarkably good over a large radial interval. In addition, Newtonian models are isotropic in the central regions, while dMOND models are radially anisotropic down to the center.

2) In NLC we found that final states of full MOND models, if interpreted in the context of Newtonian gravity, are characterized by a *dividing radius* of the order of R_e , separating a baryon-dominated inner region from a dark-matter dominated outer region, in accordance^{36,37} with observations of elliptical galaxies. However, we were not able to reproduce the observed scaling laws of elliptical galaxies *under the assumption of a luminosity-independent stellar mass-to-light ratio*.

3) Phase mixing is less effective (and stellar systems take longer to relax) in MOND than in Newtonian gravity. This behavior is confirmed by numerical simulations in which the angular force components are frozen to zero, so possible differences in radial orbit instability between Newtonian and MOND gravity are not relevant in the present context. Our results on mixing suggest that merging could take longer in MOND than in Newtonian gravity; on the other hand, analytical estimates of the two-body relaxation time seem to indicate³⁸ the opposite, predicting shorter dynamical friction time-scales in MOND than in Newtonian gravity: the next application of our code will be the study of galaxy merging in MOND.

Acknowledgments

We are grateful to Giuseppe Bertin, James Binney, and Scott Tremaine for helpful discussions, and to Italian MIUR for the grant CoFin2004.

References

1. C. Nipoti, P. Londrillo, & L. Ciotti, *astro-ph* 0701418 (2007), (NLC).
2. J. Bekenstein, & M. Milgrom, *ApJ* **286**, 7 (1984).
3. M. Milgrom, *ApJ* **270**, 365 (1983).
4. R. Brada, & M. Milgrom, *MNRAS* **276**, 453 (1995).
5. L. Ciotti, P. Londrillo, & C. Nipoti, *ApJ* **640**, 741 (2006).
6. J.E. Felten, *ApJ* **286**, 3 (1984).
7. M. Milgrom, *New. Astron. Rev.* **46**, 741 (2002).

8. R.H. Sanders, & S.S. McGaugh, *ARAA* **40**, 263 (2002).
9. J. Bekenstein, *Phys. Rev. D* **70**, 083509
10. R. Brada, & M. Milgrom, *ApJ* **519**, 590 (1999).
11. R. Brada, & M. Milgrom, *ApJ* **541**, 556 (2000).
12. S. Stachniewicz, & M. Kutschera, *MNRAS* **362**, 89 (2005).
13. A. Nusser, & E. Pointecouteau, *MNRAS* **366**, 96 (2006).
14. O. Turet, & F. Combes, *astro-ph* 0701011, (2007).
15. P. Londrillo, C. Nipoti, & L. Ciotti, *Mem. S.A.It. Supplement* **1**, 18 (2003).
16. C. Nipoti, P. Londrillo, & L. Ciotti, *MNRAS* **342**, 501 (2003).
17. J. Binney, & S. Tremaine, *Galactic Dynamics* (Princeton University Press: Princeton, 1987).
18. L. Ciotti, *Lecture Notes on Stellar Dynamics* (Scuola Normale Superiore: Pisa, 2001).
19. M. Milgrom, *ApJ* **287**, 571 (1984).
20. O.E. Gerhard, D.N. Spergel, *ApJ* **397**, 38 (1992).
21. M. Milgrom, *ApJ* **429**, 540 (1994).
22. H.C. Plummer, *MNRAS* **71**, 460 (1911).
23. C. Nipoti, P. Londrillo, & L. Ciotti, *MNRAS* **332**, 901 (2002).
24. C. Nipoti, P. Londrillo, & L. Ciotti, *MNRAS* **370**, 681 (2006).
25. W. Dehnen, *MNRAS* **265**, 250 (1993).
26. S. Tremaine, et al., *AJ* **107**, 634 (1994).
27. J.L. Sersic, *Atlas de galaxias australes* (Obs. Astron., Cordoba, 1968).
28. L. Ciotti, *A&A* **249**, 99 (1991).
29. L. Ciotti, & G. Bertin, *A&A* **352**, 447 (1999).
30. G. Bertin, L. Ciotti, L., & M. Del Principe, *A&A* **386**, 1491 (2002).
31. D. Lynden-Bell, *MNRAS* **136**, 101 (1967).
32. T.S. van Albada, *MNRAS* **201**, 939 (1982).
33. J. Binney, *MNRAS* **200**, 951 (1982).
34. P. Londrillo, A. Messina, & M. Stiavelli, *MNRAS* **250**, 54 (1991).
35. M. Trenti, G. Bertin, & T.S. van Albada, *A&A* **433**, 57 (2005).
36. G. Bertin, et al., *A&A* **292**, 381 (1994).
37. M. Cappellari, et al., *MNRAS* **366**, 1126 (2006).
38. L. Ciotti, & J. Binney, *MNRAS* **351**, 285 (2004).